

$D^+ \rightarrow K^- \pi^+ \pi^+$: The weak vector current

P. C. Magalhães* and M. R. Robilotta

Instituto de Física, Universidade de São Paulo, São Paulo, São Paulo, 05508-090, Brazil

(Received 23 April 2015; published 3 November 2015)

Studies of D and B meson decays into hadrons have been used to test the standard model in the last 15 years. A heavy meson decay involves the combined effects of a primary weak vertex and subsequent hadronic final-state interactions, which determine the shapes of Dalitz plots. The fact that final products involve light mesons indicates that the QCD vacuum is an active part of the problem. This makes the description of these processes rather involved and, in spite of its importance, phenomenological analyses tend to rely on crude models. Our group produced, some time ago, a schematic calculation of the decay $D^+ \rightarrow K^- \pi^+ \pi^+$, which provided a reasonable description of data. Its main assumption was the dominance of the weak vector current, which yields a nonfactorizable interaction. Here we refine that calculation by including the correct momentum dependence of the weak vertex and extending the energy ranges of $\pi\pi$ and $K\pi$ subamplitudes present into the problem. These new features make the present treatment more realistic and bring theory closer to data.

DOI: 10.1103/PhysRevD.92.094005

PACS numbers: 13.25.Ft, 11.80.Jy, 13.75.Lb

I. MOTIVATION

Nonperturbative QCD calculations are difficult and can only be performed in approximate frameworks. The grouping of quarks into two sets, according to their masses, provides a convenient point of departure for approximations. Quarks u , d , and s can be considered as light and quarks c , b , and t as heavy, even though the s -quark is not too light and the c -quark is not too heavy. This approach is useful because light quark condensates are active close to the ground state of QCD and give rise to highly collective interactions.

Pions and kaons are the most prominent light quark systems, but data available for elastic $K\pi$ scattering are scarce and decades old. They were obtained from the LASS spectrometer at SLAC [1,2], in the range $0.825 < \sqrt{s} < 1.960$ GeV, by isolating one-pion exchanges in the reaction $KN \rightarrow \pi KN$. In the last ten years, information about $K\pi$ interactions was also produced by hadronic decays of D mesons. In particular, data from the E791 and FOCUS collaborations [3,4] for the reaction $D^+ \rightarrow K^- \pi^+ \pi^+$ allowed the S -wave $K\pi$ subamplitude to be extracted continuously from threshold up to the high-energy border of the Dalitz plot. Hope was then raised that these data could improve the description of elastic $K\pi$ scattering. However, decay data differ significantly from those given by the LASS experiment and this discrepancy motivates our interest in this problem.

The description of the decay $D^+ \rightarrow K^- \pi^+ \pi^+$ must include both the weak $c \rightarrow s$ vertex and hadronic final-state interactions (FSIs), which correspond to strong processes occurring between primary decay and detection. The study of weak vertices departs from the topological

structures given by Chau [5], which implement Cabbibo-Kobayashi-Maskawa quark mixing for processes involving a single W . As primary decays occur in the presence of light quark condensates, the direct incorporation of Chau's scheme into calculations is not trivial and one is forced into hadronic descriptions. Dominant contributions to D decay may be accounted for by the effective Lagrangian proposed by Bauer *et al.* [6], which reads

$$L_{\text{eff}} = \frac{G_F}{\sqrt{2}} \{a_1 (\bar{u}d')_H (\bar{s}'c)_H + a_2 (\bar{s}'d')_H (\bar{u}c)_H\}, \quad (1)$$

where a_i are the Wilson coefficients and $(\bar{u}d')_H$ and $(\bar{s}'c)_H$ are the factorized quark currents, related, respectively, to the matrix $\langle H(\bar{u}d)|(A-V)^\mu|0\rangle$ and $\langle H(s)|(A-V)^\mu|D\rangle$. This factorization technique was employed in the $D^+ \rightarrow K^- \pi^+ \pi^+$ study by Boito and Escribano [7] with a quasi-two-body model for the FSI. Concerning the treatment of relativistic final-state interactions, high-energy few-body calculations have begun to be available now [8–10] and several works have already employed field theory to FSIs in heavy meson decays [7,11–17].

In this work, the decay $D^+ \rightarrow K^- \pi^+ \pi^+$ is treated by means of chiral effective Lagrangians, supplemented by phenomenological form factors. This framework is motivated by the smallness of the u , d , and s masses, when compared with the QCD scale $\Lambda \sim 1$ GeV. The light sector of the theory is therefore not far from the massless limit, which is symmetric under the chiral $SU(3) \times SU(3)$ flavor group. In this approach, light condensates arise naturally and pseudoscalar mesons are described as Goldstone bosons. Quark masses are incorporated perturbatively into effective Lagrangians [18,19], whereas weak interactions are treated as

*patricia@if.usp.br

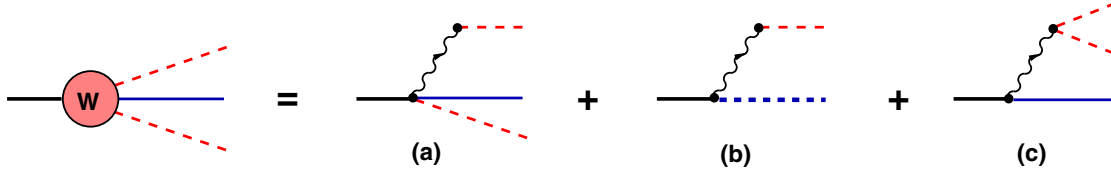


FIG. 1 (color online). Topologies for the weak vertex. The dotted line is a scalar resonance and the wavy line is the W^+ , which is contracted to a point in calculations.

external sources. Chiral perturbation theory was originally designed to describe low-energy interactions, where it yields the most reliable representation of QCD available at present. Its scope was later enlarged, with the inclusion of resonances as chiral corrections [20], and the unitary resummation of diagrams [21]. Suitable coupling schemes also allow the incorporation of heavy mesons [22] and the final effective Lagrangians are able to describe both energy sectors.

A similar theoretical framework has already been employed by our group [16], in an exploratory study of FSI in $D^+ \rightarrow K^- \pi^+ \pi^+$. With the purpose of taming an involved calculation, in that work we made a number of simplifying assumptions. Among them, the weak vertices were taken to be constants, isospin 3/2 and P waves were not included in intermediate $K\pi$ amplitudes, and couplings to either vector mesons or inelastic channels were neglected. In spite of these limitations, that work allowed the identification of leading dynamical mechanisms and gave rise to results which are reasonable for the modulus and good for the phase of the S -wave $K\pi$ subamplitude [3,4]. In this work, we focus on the vector weak amplitude and improve the description of the weak vertex, by including both the correct momentum dependence and better phenomenology for an intermediate $\pi\pi$ subamplitude, and the description of a $K\pi$ subamplitude at higher energies. These new features tend to reduce the gap between theory and experiment.

II. DYNAMICS

We denote by $[K^- \pi^+]_S$ the S -wave $K^- \pi^+$ subamplitude in the decay $D^+ \rightarrow K^- \pi^+ \pi^+$, which has been extracted by the E791 [3] and FOCUS [4] collaborations. The decay begins with the primary quark transition $c \rightarrow s W^+$, which is subsequently dressed into hadrons, owing to the surrounding light quark condensate. In the absence of form factors, this structure gives rise to the color allowed process shown in Fig. 1, where (a) and (b) involve an axial current and (c) contains a vector current. As one of the pions in diagram (c) is neutral, it does not contribute at tree level.

Inclusion of final-state interactions, due to successive elastic $K\pi$ scatterings [16], yields three families of diagrams, as in Fig. 2. It is worth noting that these series *do not* represent a loop expansion, because loops are also present within the $K\pi$ amplitude. The W^+ is shown explicitly, just to indicate the various topologies, and becomes pointlike in calculations. A family of FSI ends the forward propagating resonance in Fig. 1(b) with a dynamical width [23]. Processes involving resonances in $D^+ \rightarrow K^- \pi^+ \pi^+$ axial current decay have already been considered in Refs. [14,15,17], whereas quasi-two-body axial FSI were discussed in Ref. [7]. The general form of the vertex $\langle K^- \pi^+ | A^\mu | D^+ \rangle$ was defined by Kuhn and Mirkes [24]. When multiplied by $\langle \pi^+ | A_\mu | 0 \rangle$, the corresponding amplitude becomes proportional to $M_\pi^2 F_4$, where F_4 is a form factor. As the pion mass is very small and effective theories

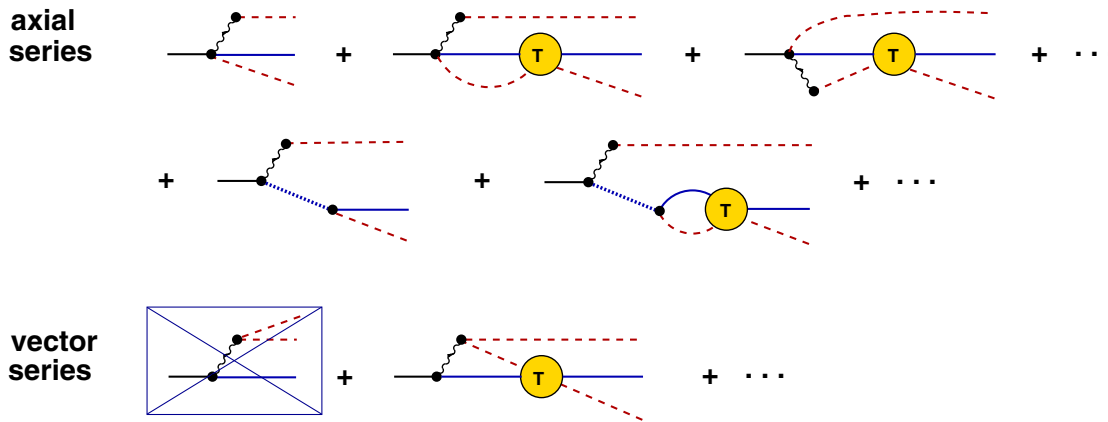


FIG. 2 (color online). Final-state interactions starting from the axial weak vertex (axial series) and from the vector weak vertex (vector series). In the former, the pion plugged in to the W^+ is always positive, whereas the \bar{K} inside the loop can be either positive or neutral in the latter, the tree diagram does not contribute, since one of the pions plugged in to the W^+ is neutral.

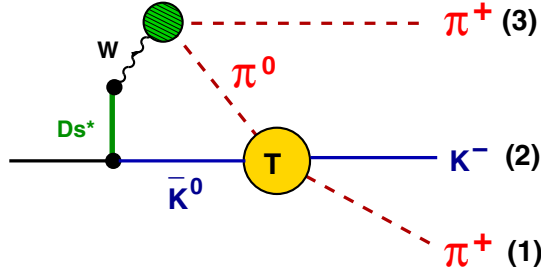


FIG. 3 (color online). Leading vector current contribution, dressed by form factors and $\pi\pi$ interactions (in the small green blob).

cannot give rise to a large F_4 , this contribution is expected to be small, as stressed in Ref. [25].

An important lesson drawn from our previous study [16] is that, for some yet unknown reason, the vector weak amplitude, represented by diagram (c) of Fig. 1, seems to be favored by data [4]. This amplitude receives no contribution at tree level, since the W^+ emitted by the c -quark decays into a $\pi^+\pi^0$ pair. Therefore, leading terms in this process necessarily involve loops, which bring imaginary components into the amplitude.

The first nonvanishing contribution to the vector series is given in Fig. 3. As the W is very heavy, one keeps just hadronic propagators, which render loop integrals finite. Denoting by A_0 the amplitude for the process $D^+ \rightarrow K^0 \pi^0 \pi^+$ without FSIs and by $T_{K\pi}$ that for $\pi^0 \bar{K}^0 \rightarrow \pi^+ K^-$, the amplitude A_1 of Fig. 3 can be schematically written as

$$A_1 = -i \int \frac{d^4 \ell}{(2\pi)^4} T_{K\pi}^S \Delta_\pi \Delta_K A_0, \quad (2)$$

$$A_1^S(m_{12}^2) = -i [G_F \cos^2 \theta_C F_1^{DK}(0)] \left[\frac{\sqrt{2}}{3} T_{K\pi}^S(m_{12}^2) \right] \int \frac{d^4 \ell}{(2\pi)^4} \frac{1}{D_\pi D_K} \frac{m_\rho^2}{D_\rho} \times \left\{ [M_D^2 + 2M_\pi^2 + M_K^2 - 2m_{12}^2 - \ell^2 + D_\pi + D_K] \frac{m_V^2}{D_V} + D_\pi (M_D^2 - M_K^2) \left[\frac{1}{D_V} - \frac{1}{D_S} \right] \right\}, \quad (4)$$

where G_F is the Fermi constant θ_C is the Cabibbo angle $F_1^{DK}(0)$ is a coupling constant [26] and the factor $\sqrt{2}/3$ is associated with the transition $K^0 \pi^0 \rightarrow K^- \pi^+$, whereas $D_\pi = [(\ell - p_3)^2 - M_\pi^2]$, $D_K = [(\ell - P)^2 - M_K^2]$,

where ℓ is the loop variable, Δ_π and Δ_K are pion and kaon propagators, and A_0 is the tree level amplitude, given by

$$A_0 = -\frac{1}{\sqrt{2}} [G_F \cos^2 \theta_C F^{DK}(0)] \langle \pi^+ \pi^0 | V_\mu | 0 \rangle \langle \bar{K}^0 | V^\mu | D^+ \rangle, \quad (3)$$

derived in Appendix B, Eq. (B17). It is worth noting that this amplitude has the same structure as those based on factorization techniques [6], presented in Eq. (1). The matrix element $\langle \bar{K}^0 | V^\mu | D^+ \rangle$ describes the $D \rightarrow W \bar{K}$ vertex, Eq. (B13), including D_s^* intermediate states [26], and corresponds to form factors parametrized in terms of vector and scalar nearest poles, Eq. (B14). The factor $\langle \pi^+ \pi^0 | V_\mu | 0 \rangle$ is associated with the process $W \rightarrow \pi\pi$, shown in Fig. 4, and includes the ρ with a dynamical width, Eq. (B10). The bare resonance is treated by employing the formalism developed in Ref. [20] and its width is constructed using the P -wave elastic $\pi\pi$ amplitude.

The $W \rightarrow \pi\pi$ form factor is timelike and its inclusion into the vector series of Fig. 2 can, in principle, give rise to final-state interactions depending on both $\pi\pi$ and $K\pi$ amplitudes. With the purpose of keeping complications to a minimum, we consider just $\pi\pi$ interactions that occur before the first $K\pi$ scattering.

The evaluation of Fig. 3 requires the $K\pi$ amplitude in the interval $0.401 \text{ GeV}^2 \leq s \leq 2.993 \text{ GeV}^2$. As LASS data [1] begin only at $s = 0.681 \text{ GeV}^2$, one covers the low-energy region by means of theoretical amplitudes, based on unitarized chiral symmetry [20]. Our intermediate S -wave $K\pi$ amplitude, denoted by $T_{K\pi}^S$, is thoroughly discussed in Appendix C.

Using the results of (B17) in Eq. (2), one finds

$D_V = [\ell^2 - m_V^2]$, $D_S = [\ell^2 - m_S^2]$, in which the subscripts V and S stand for the $D_s^*(2112)$ and $D_{s0}^*(2317)$ states. Finally, D_ρ is a complex function defined by Eqs. (B15) and (B16). This structure yields

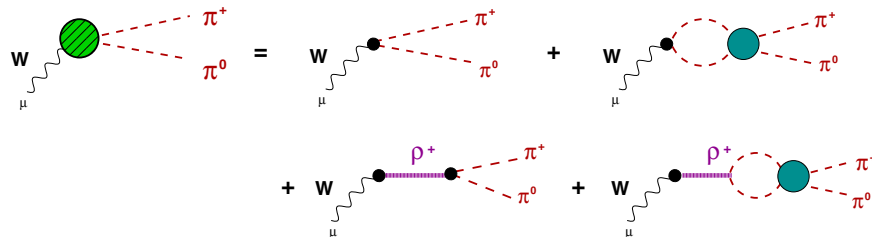
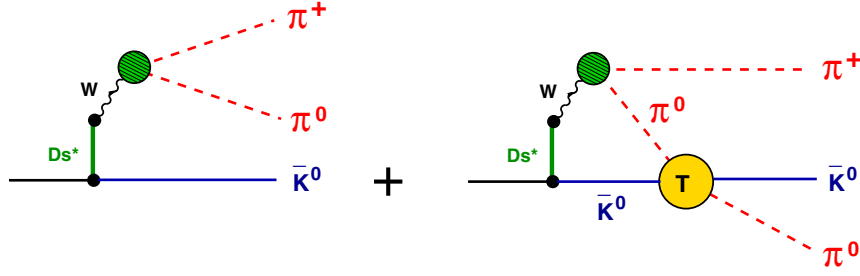


FIG. 4 (color online). Structure of the $W \rightarrow \pi\pi$ form factor. The blue blob is the elastic $\pi\pi$ amplitude.

FIG. 5 (color online). Vector current diagrams contributing to the decay $D^+ \rightarrow \bar{K}^0 \pi^0 \pi^+$.

$$A_1^S(m_{12}^2) = -i\alpha \frac{\sqrt{2}}{3} \left[\frac{T_{K\pi}^S(m_{12}^2)}{16\pi^2} \right] \times \{ \beta I_{\pi K\rho V}^S - I_{\pi KV}^S + I_{\pi\rho V}^S + I_{K\rho V}^S - \gamma I_{K\rho VS}^S \}, \quad (5)$$

with

$$\alpha = [G_F \cos^2 \theta_C F_1^{DK}(0)] m_\rho^2 m_V^2, \quad (6)$$

$$\beta = M_D^2 + 2M_\pi^2 + M_K^2 - m_\rho^2 - 2m_{12}^2, \quad (7)$$

$$\gamma = -(M_D^2 - M_K^2)(m_V^2 - m_S^2)/m_V^2, \quad (8)$$

and I_{abcd}^S, I_{abcd}^S are the loop integrals

$$I_{abc}^S = \int \frac{d^4 \ell}{(2\pi)^4} \frac{16\pi^2}{D_a D_b D_c},$$

$$I_{abcd}^S = \int \frac{d^4 \ell}{(2\pi)^4} \frac{16\pi^2}{D_a D_b D_c D_d}. \quad (9)$$

The form of these integrals are discussed in Appendix D.

III. VECTOR FSI SERIES

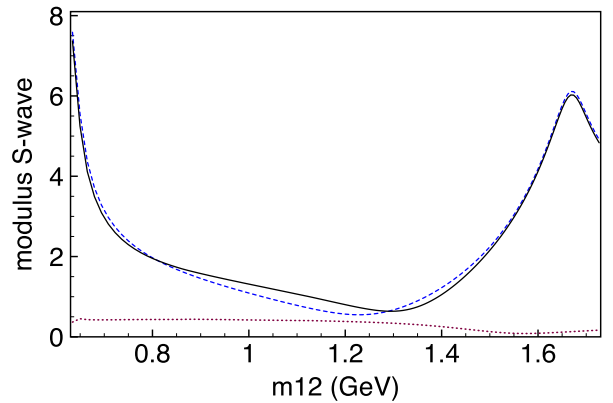
In the decay $D^+ \rightarrow K^- \pi^+ \pi^+$, there is no tree contribution to the vector FSI series, as in Fig. 2. However, before moving into this reaction, it is instructive to assess the relative importance of allowed tree and one-loop contributions in the decay $D^+ \rightarrow \bar{K}^0 \pi^0 \pi^+$, indicated in Fig. 5. The amplitude describing the left diagram is denoted by A_0 , the tree amplitude defined in Eq. (3) and with final form given in Eq. (B17). Projecting out the S -wave, we find

$$A_0^S = -[G_F \cos^2 \theta_C F_1(0)] \sum_i \left\{ \frac{m_V^2 N_i}{m_V^2 - \theta_i} \times [(M_D^2 + 2M_\pi^2 + M_K^2 - 2m_{12}^2 - m_V^2) \Pi_V - (M_D^2 + 2M_\pi^2 + M_K^2 - 2m_{12}^2 - \theta_i) \Pi_{\theta_i}] \right\}, \quad (10)$$

$$\Pi_{[V;\theta_i]} = \frac{1}{2\beta} \ln \frac{[m_V^2; \theta_i] - \alpha_{13}^2 - \beta}{[m_V^2; \theta] - \alpha_{13}^2 + \beta}, \quad (11)$$

where θ_i and N_i are complex parameters given in Table I (Appendix B) and $m_V = m_{D^*(2112)}$. The first order amplitude is obtained by replacing the isospin factor $\sqrt{2}/3$ with $-1/3$ in Eq. (5).

Results for the moduli from tree and one-loop contributions, displayed in Fig. 6, indicate a clear dominance of the former. The main structural difference between both terms is the factor $\{T_{K\pi}^S/48\pi^2\}$ in the latter, associated with a final-state scattering. Its scale can be understood by noting that chiral symmetry predicts this amplitude to be $T_{K\pi}^S = 2M_\pi M_K/F^2 \sim 13$ at threshold whereas LASS data [1] indicate that it reaches a maximum of $T_{K\pi}^S \sim 50$ around $m_{12} \sim 1.33$ GeV. Therefore the factor $\{T_{K\pi}^S/48\pi^2\}$ is always smaller than $1/10$ and pushes down the loop contribution. This result can be taken as an indication that the vector series, as given in Fig. 2, converges rapidly. The confirmation of this hint depends, of course, on the explicit calculation of next terms in the series.

FIG. 6 (color online). Modulus of the $D^+ \rightarrow \bar{K}^0 \pi^0 \pi^+$ amplitude (full line) and partial contributions from tree [Eq. (10)] (dashed line) and one loop (dotted line).

IV. RESULTS: S-WAVE

One of the purposes of this work is to understand the role played by the high-energy components of intermediate $\pi\pi$ and $K\pi$ subamplitudes in the description of data. Predictions from Eq. (5) for the phase and modulus of $[K^- \pi^+]_S$, the S -wave $K^- \pi^+$ subamplitude in $D^+ \rightarrow K^- \pi^+ \pi^+$, are given in Figs. 7 and 8.

As far as the $\pi\pi$ subsystem is concerned, the data of Hyams *et al.* [27] are used in a parametrized form, in the whole region of interest, as discussed in Appendix B. For the sake of producing a contrast, we also show curves corresponding to

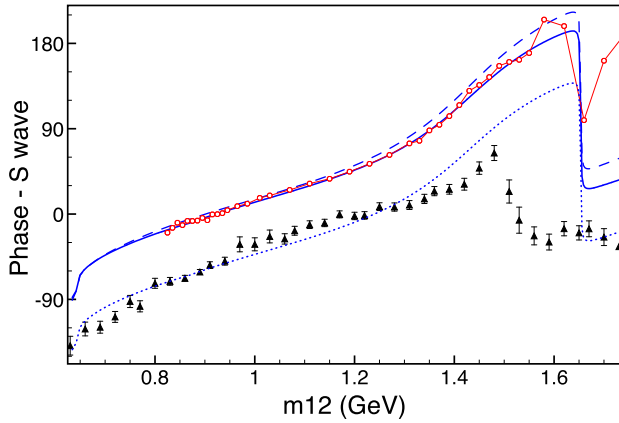


FIG. 7 (color online). Predictions for the $D^+ \rightarrow K^- \pi^+ \pi^+$ phase (full blue curve), based on the parametrized $\pi\pi$ and $K\pi$ amplitudes given in Appendixes B and C, compared with FOCUS data [4]. The blue dotted curve is the previous one shifted by -55° the dashed blue curve is based on the one- ρ pole approximation for the $\pi\pi$ amplitude in the red symbol continuous curve the *hybrid* model was used for the $K\pi$ amplitude.

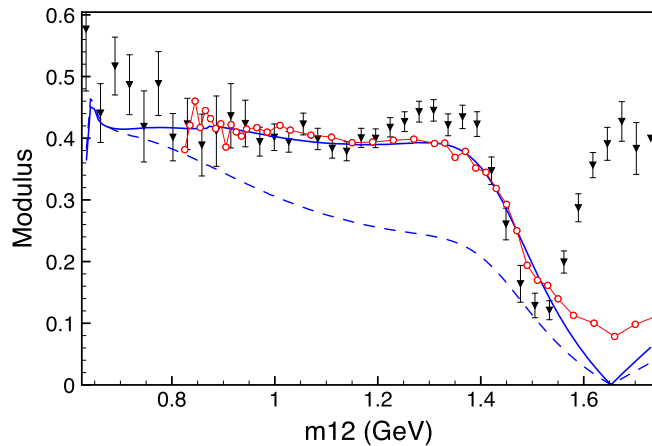


FIG. 8 (color online). Predictions for $D^+ \rightarrow K^- \pi^+ \pi^+$ modulus (full blue curve), based on the parametrized $\pi\pi$ and $K\pi$ amplitudes given in Appendixes B and C, compared with FOCUS data [4], using arbitrary normalization. The dashed blue curve is based on the one- ρ pole approximation for the $\pi\pi$ amplitude in the red symbol continuous curve the *hybrid* model was used for the $K\pi$ amplitude.

the low-energy vector-meson-dominance approximation, in which the P -wave amplitude is described by just an intermediate ρ -meson, which amounts to using just the first term in Eq. (B16). In the case of the $K\pi$ amplitude, data are not available for energies below 0.825 GeV [1] and two alternative extensions are given in Appendix C. One of them is based on a two-resonance fit, which encompasses both low- and high-energy sectors, whereas in the other one LASS data [1] are used directly, when available, and extrapolated to the threshold region by means of a fit, based on a unitarized chiral symmetry structure. In the sequence we refer to these versions as *fitted* and *hybrid*, respectively. The main difference between them is that the former excludes data points around $E \sim 1.7$ GeV, shown in Fig. 10, where two-body unitarity is violated.

Inspecting the figures, one learns that the improvement in $\pi\pi$ phenomenology is more important for the modulus, where it influences considerably the curve behavior and increases significantly the range in energy where the theoretical description proves to be reasonable. In the case of the phase, effects associated with $\pi\pi$ phenomenology are small and visible only above $m_{12} > 1.2$ GeV. On the other hand, the use of either the fitted or hybrid $K\pi$ amplitudes produces equivalent results, except at the high-energy end, where none of them is satisfactory. This seems to indicate missing structures that could be associated with other topologies in $D^+ \rightarrow K^- \pi^+ \pi^+$ decay.

As experimental results for the FOCUS phase [4] include an arbitrary constant, in Fig. 7 we also show our main result displaced by -55° . One notices an overall good agreement with data, from threshold up to $m_{12} \sim 1.4$ GeV. As our results were based on the vector series shown in Fig. 2, which does not contain a tree contribution, there are two sources of complex phases in this problem. One of them is that associated with the $K\pi$ amplitude, whereas the other one is less usual and due to the loop including the weak vertex. Our results indicate that the latter is rather important over the whole energy range considered. This shows the relevance of proper three-body interactions, which share the initial momentum with all final particles at once.

V. CONCLUSIONS

In this work we calculate the weak vector current contribution to the process $D^+ \rightarrow K^- \pi^+ \pi^+$, employing intermediate $\pi\pi$ and $K\pi$ intermediate subamplitudes valid within most of the Dalitz plot. Together with the use of a proper P -wave weak vertex, this extends a previous study made on the subject [16]. We still concentrate on $[K^- \pi^+]_S$, the S -wave $K^- \pi^+$ subamplitude, and present predictions for both the phase and modulus, given by the blue curves in Figs. 7 and 8, that are quite satisfactory from threshold to 1.4 GeV. Results for the modulus, in particular, improve considerably from our previous findings, showing that intermediate $\pi\pi$ subamplitudes are important and need to be treated carefully. As far as the phase is concerned, the

most prominent feature is the fact that it has a large negative value at threshold. In QCD, loops are the only source of complex amplitudes and, in this problem, the energy available in the loop of Fig. 3 can be larger than both $K\pi$ and $K\rho$ thresholds. This yields a rich complex structure for the loop containing the W , with a phase Θ_L which adds to the phase $\Theta_{K\pi}$ already present in the intermediate $K\pi$ amplitude. Therefore Θ_L represents the gap between the two- and three-body phases, which depends on both m_{12} and m_{23} , showing that Watson's theorem does not apply to this case.

On general grounds, the weak process in the $D^+ \rightarrow K^- \pi^+ \pi^+$ decay is known to include both axial and vector contributions. In this work we concentrated on the latter, leaving the evaluation of the axial vertex to a future work, even expecting it to give a small contribution, proportional to M_π^2 . Nevertheless, our present results both confirm the importance of weak vector currents in this branch of D^+ decays and indicate that proper three-body final-state interactions, in which the initial four-momentum of the D^+ is shared among all final particles, are rather visible over the whole energy range considered. This is consistent with the dominance of weak vector currents observed experimentally in the $D^+ \rightarrow \bar{K}^0 \pi^0 \pi^+$ decay [28]. In a parallel study, to be presented elsewhere, we found that this feature is also present in the P -wave projection of final-state $K\pi$ subamplitude, which has a nonvanishing phase at threshold.

ACKNOWLEDGEMENTS

The work of P. C. M. was supported by Fundação de Amparo à Pesquisa do Estado de São Paulo (FAPESP).

APPENDIX A: KINEMATICS

The momentum of the D -meson is P , whereas those of the outgoing kaon and pions are p_2 , p_1 , and p_3 , respectively. The invariant masses read

$$m_{12}^2 = (p_1 + p_2)^2 = M_\pi^2 + M_K^2 + 2p_1 \cdot p_2, \quad (\text{A1})$$

$$m_{13}^2 = (p_1 + p_3)^2 = 2M_\pi^2 + 2p_1 \cdot p_3, \quad (\text{A2})$$

$$m_{23}^2 = (p_2 + p_3)^2 = M_\pi^2 + M_K^2 + 2p_2 \cdot p_3, \quad (\text{A3})$$

and satisfy the constraint

$$M_D^2 = m_{12}^2 + m_{13}^2 + m_{23}^2 - 2M_\pi^2 - M_K^2. \quad (\text{A4})$$

The projection into partial waves for subsystem (12) is performed by going to its center of mass and writing

$$m_{13}^2 = \alpha_{13}^2 - \beta_{12} \cos \theta, \quad (\text{A5})$$

$$m_{23}^2 = \alpha_{23}^2 + \beta_{12} \cos \theta, \quad (\text{A6})$$

$$\alpha_{13}^2 = [M_D^2 + 2M_\pi^2 + M_K^2 - m_{12}^2 - (M_D^2 - M_\pi^2)(M_K^2 - M_\pi^2)/m_{12}^2]/2, \quad (\text{A7})$$

$$\alpha_{23}^2 = [M_D^2 + 2M_\pi^2 + M_K^2 - m_{12}^2 + (M_D^2 - M_\pi^2)(M_K^2 - M_\pi^2)/m_{12}^2]/2, \quad (\text{A8})$$

$$\beta_{12} = 2Q'q', \quad (\text{A9})$$

$$q' = \frac{1}{2\sqrt{m_{12}^2}} [m_{12}^4 - 2(M_\pi^2 + M_K^2)m_{12}^2 + (M_\pi^2 - M_K^2)^2]^{1/2}, \quad (\text{A10})$$

$$Q' = \frac{1}{2\sqrt{m_{12}^2}} [m_{12}^4 - 2(M_\pi^2 + M_D^2)m_{12}^2 + (M_\pi^2 - M_D^2)^2]^{1/2}, \quad (\text{A11})$$

where θ is the angle between the momenta of the pions.

APPENDIX B: BASIC $D^+ \rightarrow \bar{K}^0 \pi^0 \pi^+$ AMPLITUDE

Our description of the decay $D^+ \rightarrow K^- \pi^+ \pi^+$ includes both the primary weak vertex and hadronic final-state interactions, associated with successive $K\pi$ scatterings. When the $W \rightarrow \pi\pi$ vertex is corrected by means of timelike form factors, both the ρ -meson and P -wave $\pi\pi$ interactions also become part of the problem. This could, in principle, give rise to a structure of final interactions depending on both $\pi\pi$ and $K\pi$ amplitudes. Therefore, the amplitude for the process $D^+(P) \rightarrow \bar{K}^0(p_K)\pi^0(p_0)\pi^+(p_+)$ at tree level, given in Fig. 5 (left) and denoted by A_0 , becomes the basic building block in the evaluation of the weak vector series. As it includes the $W \rightarrow \pi\pi$ form factor, we consider the following steps:

1. Construction of the $\pi\pi$ amplitude

The diagrams of Fig. 4 depend on $T_{\pi\pi}^{P1}$, the $I = 1$, P -wave $\pi\pi$ amplitude. The momenta of the outgoing pions are p_+ and p_0 , whereas those inside the two-pion loop are q_+ and q_0 . The total momentum is $Q = (p_+ + p_0) = (q_+ + q_0)$ and the loop integration variable is $\ell = (q_+ - q_0)/2$. Assuming that, at low energies, $\pi\pi$ interactions are dominated by a $\mathcal{O}(q^2)$ contact term supplemented by the $\mathcal{O}(q^4)$ ρ -pole contribution, the effective Lagrangians in Ref. [20] yield the tree contribution

$$\bar{T}^1 = (t - u) \left[\frac{1}{F^2} - \frac{2G_V^2}{F^4} \frac{s}{s - m_\rho^2} \right], \quad (\text{B1})$$

where F is the pion decay constant and G_V describes the $\rho\pi\pi$ coupling. The approximation $G_V = F/\sqrt{2} \sim 66$ MeV yields a more compact structure, given by

$$\bar{T}^1 = -\frac{(t - u)}{F^2} \frac{m_\rho^2}{s - m_\rho^2}. \quad (\text{B2})$$

For free particles in the center of mass frame, $(t - u) = (s - 4M_\pi^2) \cos \theta$ and P -wave projection gives rise to the kernel

$$\mathcal{K}^{P1} = -\frac{(s - 4M_\pi^2)}{3F^2} \frac{m_\rho^2}{s - m_\rho^2}. \quad (\text{B3})$$

The iteration of this kernel by means of intermediate two-pion states produces the unitarized amplitude [21]

$$T_{\pi\pi}^{P1} = \frac{\mathcal{K}^{P1}}{1 + \mathcal{K}^{P1} \Omega_{\pi\pi}}, \quad (\text{B4})$$

where $\Omega_{\pi\pi}$ is a divergent loop function. Therefore, we write it as the sum of an infinite constant Λ_∞ and a regular component $\bar{\Omega}_{\pi\pi}$, given by [16]

$$\bar{\Omega}_{\pi\pi} = -\frac{S}{16\pi^2} \left\{ 2 - \frac{\sqrt{\lambda}}{s} \ln \left[\frac{s - 2M_\pi^2 + \sqrt{\lambda}}{2M_\pi^2} \right] + i\pi \frac{\sqrt{\lambda}}{s} \right\},$$

$$\lambda = s^2 - 4sM_\pi^2, \quad (\text{B5})$$

where $S = 1/2$ is the symmetry factor for identical particles. After regularization, one finds

$$T_{\pi\pi}^{P1} = \frac{\mathcal{K}^{P1}}{1 + \mathcal{K}^{P1} (\bar{\Omega}_{\pi\pi} + C_{\pi\pi})}, \quad (\text{B6})$$

where $C_{\pi\pi}$ is an arbitrary constant.

The $I = 1$ amplitude to be used in the evaluation of the $W \rightarrow \pi\pi$ vertex (Fig. 4) is given by Eq. (B6) multiplied by $(3 \cos \theta)$. It is denoted by $T_{\pi\pi}^1$ and can be cast in the covariant form

$$T_{\pi\pi}^1 = 3 \frac{(t - u)}{s - 4M_\pi^2}$$

$$T_{\pi\pi}^{P1} = -6 \frac{(p_+ - p_0)^\nu \ell_\nu}{s - 4M_\pi^2} T_{\pi\pi}^1. \quad (\text{B7})$$

2. Construction of the $W \rightarrow \pi\pi$ vertex

The diagrams of Fig. 4 correspond to the following matrix element of the vector current V_μ :

$$\langle \pi^+ \pi^0 | V_\mu | 0 \rangle = -\sqrt{2} \left[\frac{m_\rho^2}{Q^2 - m_\rho^2} \right]$$

$$\times \left[(p_+ - p_0)_\mu + i6 \frac{(p_+ - p_0)^\nu}{Q^2 - 4M_\pi^2} T_{\pi\pi}^{P1}(Q^2) I_{\mu\nu} \right],$$

$$I_{\mu\nu} = \int \frac{d^4 \ell}{(2\pi)^4} \frac{\ell_\mu \ell_\nu}{[(\ell + Q/2)^2 - M_\pi^2][(\ell - Q/2)^2 - M_\pi^2]}. \quad (\text{B8})$$

The regular part of $I_{\mu\nu}$ can be related with Eq. (B5), and one has [29,30]

$$I_{\mu\nu} = \frac{i}{6} [Q^2 - 4M_\pi^2] \left[g_{\mu\nu} - \frac{Q_\mu Q_\nu}{Q^2} \right] [\bar{\Omega}_{\pi\pi} + C_{\pi\pi}] \quad (\text{B9})$$

and finds

$$\langle \pi^+ \pi^0 | V_\mu | 0 \rangle = -\sqrt{2} (p_+ - p_0)_\mu \frac{m_\rho^2}{D_\rho}, \quad (\text{B10})$$

$$D_\rho = (Q^2 - m_\rho^2) - (m_\rho^2/3F^2)(Q^2 - 4M_\pi^2)[[\bar{\Omega}_{\pi\pi} + C_{\pi\pi}]]. \quad (\text{B11})$$

3. Construction of A_0

The direct reading of the left diagram in Fig. 5 yields the tree amplitude A_0 as

$$A_0 = -\frac{1}{\sqrt{2}} [G_F \cos^2 \theta_C] \langle \pi^+ \pi^0 | V_\mu | 0 \rangle F^{DK}(0) \langle \bar{K}^0 | V^\mu | D^+ \rangle$$

$$= [G_F \cos^2 \theta_C F^{DK}(0)] (p_+ - p_0)_\mu \frac{m_\rho^2}{D_\rho} \langle \bar{K}^0 | V^\mu | D^+ \rangle, \quad (\text{B12})$$

where G_F is the Fermi constant, θ_C is the Cabibbo angle, and $F^{DK}(0) = 0.75$ [26] is the empirical phenomenological constant, and the heavy-sector vector-current matrix element is written as

$$\langle \bar{K}^0 | V^\mu | D^+ \rangle = (P_D^\mu + P_K^\mu) F_1^{DK}(Q^2)$$

$$- Q^\mu \frac{M_D^2 - M_K^2}{Q^2} [F_1^{DK}(Q^2) - F_0^{DK}(Q^2)], \quad (\text{B13})$$

where form factors are parametrized in terms of vector and scalar $c\bar{s}$ nearest poles as [26]

$$F_1(Q^2) = \frac{1}{1 - Q^2/m_V^2} \quad \text{and} \quad F_0(Q^2) = \frac{1}{1 - Q^2/m_S^2}, \quad (\text{B14})$$

with $V \rightarrow D_s^*(2100)$ and $S \rightarrow D_s^*(2317)$.

4. Tuning of A_0 to $\pi\pi$ data

The denominator D_ρ in Eq. (B12) describes the ρ meson and includes its dynamically generated width. The function D_ρ does not vanish along the real axis, in spite of the bare ρ propagators in Fig. 4. It has a zero in

TABLE I. Fitted parameters in Eq. (B16).

k	θ_R	θ_I	N_R	N_I
ρ	0.580133	-0.1137172	0.6131598	-0.1107509
1	2.539625	-0.6468928	0.2418401	-0.1080483
2	3.642091	-0.1595399	0.0016668	-0.1941643

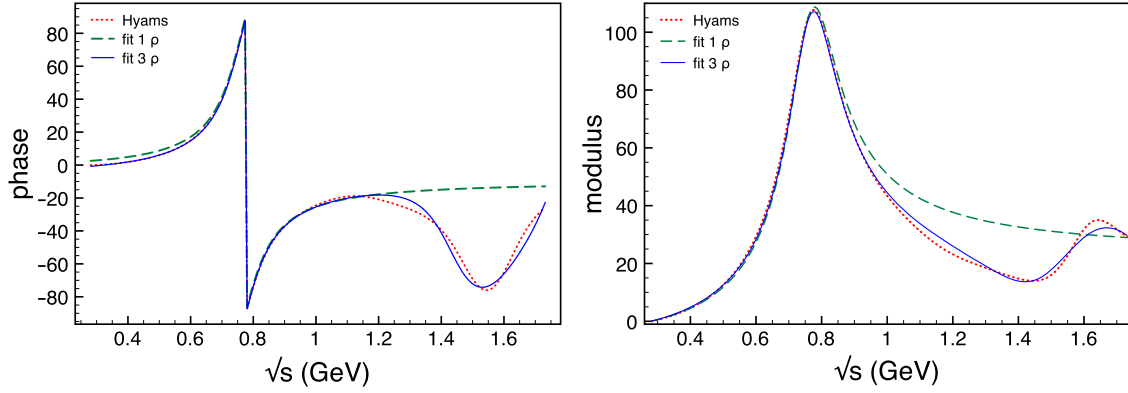


FIG. 9 (color online). Results for the $\pi\pi$ phase and modulo with only one- ρ (dashed) and adding another two poles (continuous), compared with Hyams *et al.* [27] (dotted).

the second Riemann sheet, quite close to the value quoted in Ref. [31], namely, at $Q^2 = (m_\rho - i\Gamma_\rho/2)^2$, $m_\rho = 762.4 \pm 1.8$ MeV, $\Gamma_\rho = 145.2 \pm 2.8$ MeV.

In order to simplify calculations one notes that the ratio m_ρ^2/D_ρ in Eq. (B11) is related to the P -wave amplitude, Eq. (B4), by

$$\frac{m_\rho^2}{D_\rho} = -\frac{3F^2}{s - 4M_\pi^2} T_{\pi\pi}^{P1}. \quad (\text{B15})$$

Using the data from Hyams *et al.* [27] for $T_{\pi\pi}^{P1}$, we fitted this ratio using the structure

$$\frac{m_\rho^2}{D_\rho} = \frac{N_\rho}{s - \theta_\rho} + \frac{N_1}{s - \theta_1} + \frac{N_2}{s - \theta_2}, \quad (\text{B16})$$

with parameters $\theta_k = \theta_{kR} + i\theta_{kI}$ and $N_k = N_{kR} + iN_{kI}$ given in Table I.

In Fig. 9 we display the importance of the inclusion of higher poles in Eq. (B16) in extending the agreement with Hyams *et al.* [27] data. One thus gets an expression for A_0 to be used in calculations, which includes a compatible description of $\pi\pi$ data, written as

$$A_0 = -[G_F \cos^2 \theta_C F^{DK}(0)] \left[\frac{N_\rho}{Q^2 - \theta_\rho} + \frac{N_1}{Q^2 - \theta_1} + \frac{N_2}{Q^2 - \theta_2} \right] \left\{ [M_D^2 + 2M_\pi^2 + M_K^2 - 2(p_0 + p_K)^2 - Q^2 + (p_0^2 - M_\pi^2) + (p_K^2 - M_K^2)] \frac{m_V^2}{Q^2 - m_V^2} - (p_0^2 - M_\pi^2) \frac{(M_D^2 - M_K^2)(m_V^2 - m_S^2)}{(Q^2 - m_V^2)(Q^2 - m_S^2)} \right\}. \quad (\text{B17})$$

APPENDIX C: $K\pi$ AMPLITUDE

In this work, one needs the elastic $K\pi$ amplitude over the full Dalitz plot. As there are no data [1] available in the interval $0.401 \text{ GeV}^2 \leq s \leq 0.681 \text{ GeV}^2$, one encompasses this region with the help of a theoretical amplitude, based on the unitarized chiral symmetry. This model has been discussed in detail in Refs. [16,32] and here we just summarize its main features.

For each spin-isospin channel, the unitary amplitude T_{LI} is obtained by resumming the infinite geometric series

$$\begin{aligned} T_{LI} &= \mathcal{K}_{LI} - \mathcal{K}_{LI} [\bar{\Omega}_{K\pi} + C_{LI}] \mathcal{K}_{LI} \\ &\quad + \mathcal{K}_{LI} [\bar{\Omega}_{K\pi} + C_{LI}] \mathcal{K}_{LI} [\bar{\Omega}_{K\pi} + C_{LI}] \mathcal{K}_{LI} + \dots \\ &= \frac{\mathcal{K}_{LI}}{1 + [\bar{\Omega}_{K\pi} + C_{LI}] \mathcal{K}_{LI}}, \end{aligned} \quad (\text{C1})$$

where \mathcal{K}_{LI} is a kernel and the function $\bar{\Omega}_{K\pi}$, related with the two-meson propagator, is given by [16]

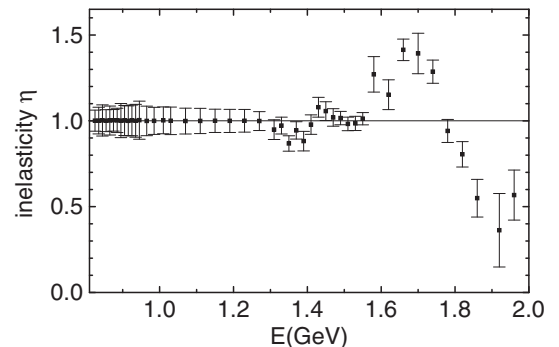


FIG. 10. Inelasticity parameter η for $S_{1/2}$ LASS data.

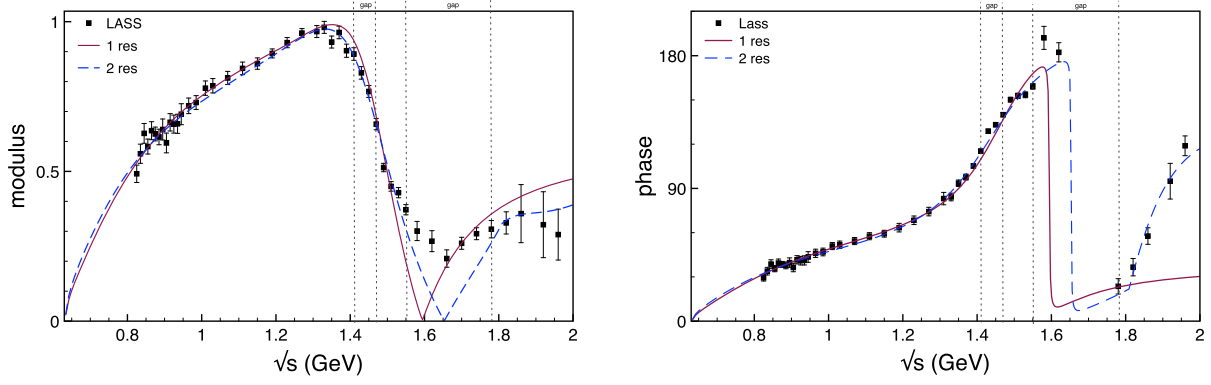


FIG. 11 (color online). Fits for the modulus and phase of the $K\pi S_{1/2}$ LASS data. Points within the regions indicated as *gap* in the top axis were excluded from the fit.

$$\begin{aligned} \bar{\Omega}_{K\pi} &= 1 + \frac{M_\pi^2 + M_K^2}{M_\pi^2 - M_K^2} \ln \frac{M_\pi}{M_K} - \frac{M_\pi^2 - M_K^2}{s} \ln \frac{M_\pi}{M_K} \\ &\quad - \frac{\sqrt{\lambda}}{s} \ln \left[\frac{s - M_\pi^2 - M_K^2 + \sqrt{\lambda}}{2M_\pi M_K} \right] + i\pi \frac{\sqrt{\lambda}}{s}, \\ \lambda &= s^2 - 2s(M_\pi^2 + M_K^2) + (M_\pi^2 - M_K^2)^2, \end{aligned} \quad (\text{C2})$$

and C_{LI} is a constant. Chiral perturbation theory determines the kernels \mathcal{K}_{LI} as the sum of an $\mathcal{O}(q^2)$ contact term [19], supplemented by $\mathcal{O}(q^4)$ corrections, which we assume to be dominated by s -, t -, and u -channel

resonances [20]. In order to fit LASS data [1], we also included a higher mass resonance, as described in Ref. [32].

In the case of the $S_{1/2}$ wave ($L, I = 0, 1/2$), the theoretical kernel is written as $\mathcal{K}_{S_{1/2}} = \mathcal{K}_{\text{BG}} + \mathcal{K}_H$, where \mathcal{K}_{BG} is a real background and \mathcal{K}_H includes resonances. The former is given by $\mathcal{K}_{\text{BG}} = \mathcal{K}_C + \mathcal{K}_S + c_V \mathcal{K}_V$, with

$$\mathcal{K}_C = \frac{1}{F^2} [s - 3q^2/2 - (M_\pi^2 + M_K^2)], \quad (\text{C3})$$

$$\begin{aligned} \mathcal{K}_S &= -\frac{4}{F^4} \{ [\bar{c}_d^2 m_0^2 - 2\bar{c}_d(\bar{c}_d - \bar{c}_m)(M_\pi^2 + M_K^2) - 2\bar{c}_d^2 q^2] + [\bar{c}_d m_0^2 - 2(\bar{c}_d - \bar{c}_m)M_\pi^2][\bar{c}_d m_0^2 - 2(\bar{c}_d - \bar{c}_m)M_K^2] I_S^t(q^2; m_0^2) \} \\ &\quad + \frac{1}{3F^4} \{ [c_d^2 m_8^2 - 2c_d(c_d - c_m)(M_\pi^2 + M_K^2) - 2c_d^2 q^2] + [c_d m_8^2 - 2(c_d - c_m)M_\pi^2][c_d m_8^2 - 2(c_d - c_m)M_K^2] I_S^t(q^2; m_8^2) \} \\ &\quad + \frac{1}{2F^4} \{ [c_d^2(m_{K^*}^2 + 2M_\pi^2 + M_K^2 - s + 2q^2) + 2c_d(c_d - c_m)(M_\pi^2 + M_K^2)] \\ &\quad + [c_d m_{K^*}^2 - (c_d - c_m)(M_\pi^2 + M_K^2)]^2 I_S^u(q^2; m_{K^*}^2) \}, \end{aligned} \quad (\text{C4})$$

$$\begin{aligned} \mathcal{K}_V &= -\left[\frac{G_V}{F^2} \right]^2 \{ [2(s - M_\pi^2 - M_K^2) + m_\rho^2 - 2q^2] + m_\rho^2 [m_\rho^2 + 2(s - M_\pi^2 - M_K^2)] I_S^t(q^2; m_\rho^2) \} \\ &\quad - \frac{1}{4} \left[\frac{G_V}{F^2} \right]^2 \{ [m_{K^*}^2 + s + 2q^2] + [m_{K^*}^2(m_{K^*}^2 + 2(s - M_\pi^2 - M_K^2)) - (M_\pi^2 - M_K^2)^2] I_S^u(q^2; m_{K^*}^2) \}, \end{aligned} \quad (\text{C5})$$

$$I_S^t(q^2; m^2) = -\frac{1}{4q^2} \ln \left[1 + \frac{4q^2}{m^2} \right], \quad (\text{C6})$$

$$I_S^u(q^2; m^2) = \frac{1}{4q^2} \ln \left[1 - \frac{4q^2}{m^2 + s - 2(M_\pi^2 + M_K^2)} \right], \quad (\text{C7})$$

where F , c_d , c_m , \bar{c}_d , \bar{c}_m , and G_V are coupling constants and the CM three-momentum is

$$q^2 = \frac{1}{4s} [s^2 - 2s(M_\pi^2 + M_K^2) + (M_\pi^2 - M_K^2)^2]. \quad (\text{C8})$$

Two s -channel resonances are incorporated as sum of Breit-Wigner functions [32]

$$\mathcal{K}_H = -\frac{3}{2F^4} \left[\frac{[c_d s - (c_d - c_m)(M_\pi^2 + M_K^2)]^2}{s - m_{K_0^*}^2 + i g_a^2 Q_a / 8\pi\sqrt{s}} + \frac{[c_{db} s - (c_{db} - c_{mb})(M_\pi^2 + M_K^2)]^2}{s - m_b^2 + i g_b^2 Q_b / 8\pi\sqrt{s}} \right], \quad (\text{C9})$$

$$g_i = A_i + B_i s, \quad (\text{C10})$$

$$Q_i = \frac{\sqrt{s}}{2} (1 - h_i^2/s). \quad (\text{C11})$$

The usual inelasticity parameter η , evaluated for $S_{1/2}$ data, is shown in Fig. 10. Points for which $\eta > 1$ within error bars were discarded in our fit.

We have extended $S_{1/2} K\pi$ data to threshold by means of two different fits. The first one includes just a single resonance and holds for energies smaller than 1.33 GeV, whereas the second one includes two resonances and is valid over the whole Dalitz plot. They correspond, respectively, to $\chi^2/\text{n.d.f.} = 0.55$ and $\chi^2/\text{n.d.f.} = 1.62$. Our parameters, in suitable powers of GeV, are $F = 1.02722$, $G_V = 0.0686287$, $m_8 = m_0 = 0.983$ and $C_{S_{1/2}} = 1.124899 \times 10^{-2}$, $m_{K_0^*} = 1.108858$, $c_d = 0.0254505$, $c_m = 0.1483455$, $A_a = 4.563646$, $B_a = -2.055842$, $h_a = 1.138489$, $c_V = 0.26200$ for the single resonance fit and $C_{S_{1/2}} = -2.273182 \times 10^{-3}$, $m_{K_0^*} = 1.338404$, $c_d = 0.026607$, $c_m = 0.017428$, $A_a = 4.952313$, $B_a = -1.956429$, $h_a = 1.130126$, $m_b = 2.003338$, $c_{db} = 0$, $c_{mb} = 0.166268$, $A_b = 5.042537$, $B_b = -7.182061$, $h_b = 1.809129$, and $c_V = 0.89272$ for the two-resonance case.

Both fits for the modulus and phase are given in Fig. 11. In the $D^+ \rightarrow K^- \pi^+ \pi^+$ decay amplitude, alternatively, we can use directly empirical data from LASS [1] and

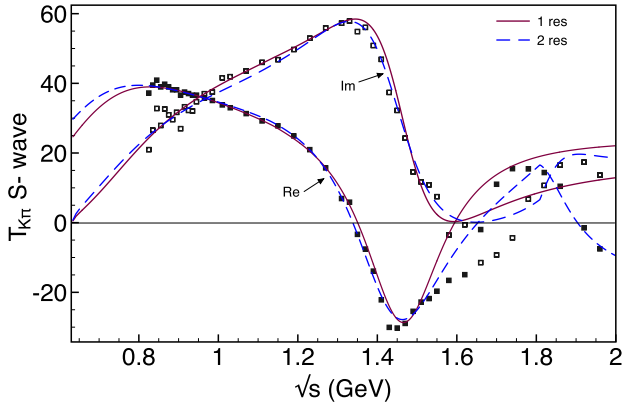


FIG. 12 (color online). Real and imaginary components of the $S_{1/2} K\pi$ amplitude fitted to LASS data (squares) and extended to low energies using chiral symmetry.

merge it with the low-energy fit, where there are no data. This became what we called *hybrid* amplitude.

In Fig. 12 we show the real and imaginary components of the amplitude. One notices that values for the real part at threshold are different, namely, 24 and 30, and they can be compared with those obtained by ChPT [33] and dispersion relations [34], respectively, $T = 21.7$ and $T = 25.5$. These values indicate that the single resonance fit is more suitable to describe low-energy behavior. Nevertheless, in the $D^+ \rightarrow K^- \pi^+ \pi^+$ calculations we consider both *hybrid* and two-resonance fits.

APPENDIX D: LOOP INTEGRALS

$$I_{abc}^S = \int \frac{d^4\ell}{(2\pi)^4} \frac{16\pi^2}{D_a D_b D_c},$$

$$I_{abcd}^S = \int \frac{d^4\ell}{(2\pi)^4} \frac{16\pi^2}{D_a D_b D_c D_d}.$$

We begin by discussing the integrals I^S , given by Eqs. (9). Their treatment can be simplified because the ρ and the $c\bar{s}$ state entering the form factor share the same momentum. This allows one to write, for instance,

$$I_{\pi K \rho V}^S = \frac{1}{M_V^2 - \Theta_R + i\Theta_I} [I_{\pi K V}^S - I_{\pi K \rho}^S], \quad (\text{D1})$$

where Θ is the parameter defined in Appendix B. Similar simplifications can be performed every time subscripts ρV or ρS occur.

The integral $I_{\pi K \rho}^S$ is important in this problem because its imaginary part is determined by two different thresholds, associated with cuts along $K\pi$ and $K\rho$ propagators. Using results from Appendix B, one writes

$$I_{\pi K \rho}^S = \int \frac{d^4\ell}{(2\pi)^4} \frac{16\pi^2}{[(\ell - p_3)^2 - M_\pi^2][(\ell - P)^2 - M_K^2]} \times \frac{N_\rho}{\ell^2 - \Theta_R + i\Theta_I}. \quad (\text{D2})$$

Representing this function by means of Feynman parameters and performing one of the integrals analytically, one finds

$$I_{\pi K \rho}^S = i N_\rho \Pi_{\pi K \rho}, \quad (\text{D3})$$

$$\Pi_{\pi K \rho} = - \int_0^1 da J_{\pi K \rho}(a), \quad (\text{D4})$$

with

$$J_{\pi K \rho}(a) = \frac{1}{\sqrt{\lambda}} \left\{ \left[\ln \frac{|F_1| |G_2|}{|G_1| |F_2|} \right] + i[\theta_J] \right\}, \quad (\text{D5})$$

$$\theta_J = [\theta_{F1} - \theta_{F2} - \theta_{G1} + \theta_{G2}], \quad (\text{D6})$$

$$F_{1,2} = \frac{|2M_D^2 a + B \mp \sqrt{\lambda}|}{M_D^2} e^{i\theta_{F1,2}}, \quad (\text{D7})$$

$$G_{1,2} = \frac{|B \mp \sqrt{\lambda}|}{M_D^2} e^{i\theta_{G1,2}}, \quad (\text{D8})$$

and

$$B = [\Theta_R - i\Theta_I - M_\pi^2 - M_K^2 + m_{12}^2 - a(M_D^2 - M_\pi^2 + m_{12}^2)], \quad (\text{D9})$$

$$\lambda = B^2 - 4M_D^2 C, \quad (\text{D10})$$

$$C = [(1-a)M_\pi^2 + aM_K^2 - a(1-a)m_{12}^2]. \quad (\text{D11})$$

The ρ width is incorporated into the factors N_ρ , Θ_I , and the case of a pointlike resonance is recovered by making $N_\rho \rightarrow 1$, $\Theta_I \rightarrow \epsilon$.

The integral $I_{\pi KV}^S$ is

$$I_{\pi KV}^S = \int \frac{d^4 \ell}{(2\pi)^4} \frac{16\pi^2}{[(\ell - p_3)^2 - M_\pi^2][(\ell - P)^2 - M_K^2]} \times \frac{1}{\ell^2 - m_V^2} = i\Pi_{\pi KV}, \quad (\text{D12})$$

and its evaluation is totally similar. However, as now $m_V > M_D$, its imaginary part comes just from the cut of the diagram along the $K\pi$ subsystem. Integrals $I_{\pi\rho V}^S$, $I_{K\rho V}^S$, and $I_{K\rho S}^S$ do not depend on m_{12}^2 .

-
- [1] D. Aston *et al.*, A study of $K^- \pi^+$ scattering in the reaction $K^+ p \rightarrow K^- \pi^+$ at 11 GeV/c, *Nucl. Phys.* **B296**, 493 (1988).
 - [2] P. Estabrooks, R. K. Carnegie, A. D. Martin, W. M. Dunwoodie, T. A. Lasinski and D. W. G. S. Leith, Study of $K\pi$ scattering using the reactions $K^\pm p \rightarrow K^\pm \pi^+ n$ and $K^\pm \pi^- \Delta^{++}$ at 13 GeV, *Nucl. Phys.* **B133**, 490 (1978).
 - [3] E. M. Aitala *et al.* (E791), Dalitz Plot Analysis of the Decay $D^+ \rightarrow K^- \pi^+ \pi^+$ and Indication of a Low-Mass Scalar $K\pi$ Resonance, *Phys. Rev. Lett.* **89**, 121801 (2002).
 - [4] J. M. Link *et al.* (FOCUS Collaboration), The $K^- \pi^+$ S-wave from the $D^+ \rightarrow K^- \pi^+ \pi^+$ decay, *Phys. Lett. B* **681**, 14 (2009).
 - [5] L.-L. Chau, Quark mixing in weak interactions, *Phys. Rep.* **95**, 1 (1983).
 - [6] M. Bauer, B. Stech, and M. Wirbel, Exclusive non-leptonic decays of D^- , D_s^- and B -mesons, *Z. Phys. C* **34**, 103 (1987).
 - [7] D. R. Boito and R. Escribano, $K\pi$ form factors and final state interactions in $D^+ \rightarrow K^- \pi^+ \pi^+$ decays, *Phys. Rev. D* **80**, 054007 (2009).
 - [8] Ya. Azimov, Quantum interference of particles and resonances, *J. Phys. G* **37**, 023001 (2010).
 - [9] K. S. F. F. Guimarães, W. de Paula, I. Bediaga, A. Delfino, T. Frederico, A. C. dos Reis, and L. Tomio, Three-body model of the final state interaction in heavy meson decay, *Nucl. Phys. B, Proc. Suppl.* **199**, 341 (2010).
 - [10] Z.-Y. Zhou, Q.-C. Wang, and Q. Gao, Investigation of the rescattering effect in D decay, *Chin. Phys. C* **35**, 708 (2011).
 - [11] I. Caprini, Rescattering effects and the σ pole in hadronic decays, *Phys. Lett. B* **638**, 468 (2006).
 - [12] B. Liu, M. Buescher, F.-K. Guo, C. Hanhart, and Ulf-G Meißner, Final state interactions in the decays $J/\psi \rightarrow VPP$, *Eur. Phys. J. C* **63**, 93 (2009).
 - [13] Ulf-G Meißner and S. Gardner, Chiral dynamics and $B \rightarrow 3\pi$ decay, *Eur. Phys. J. A* **18**, 543 (2003).
 - [14] H. Kamano, S. X. Nakamura, T.-S. H. Lee, and T. Sato, Unitary coupled-channels model for three-mesons decays of heavy mesons, *Phys. Rev. D* **84**, 114019 (2011).
 - [15] M. Diakonou and F. Diakonou, The $D^+ \rightarrow K^- \pi^+ \pi^+$ decay of the D^+ meson, *Phys. Lett. B* **216**, 436 (1989).
 - [16] P. C. Magalhães, M. R. Robilotta, K. S. F. F. Guimarães, T. Frederico, W. de Paula, I. Bediaga, A. C. dos Reis, C. M. Maekawa, and G. R. S. Zarnauskas, Towards three-body unitarity in $D^+ \rightarrow K^- \pi^+ \pi^+$, *Phys. Rev. D* **84**, 094001 (2011).
 - [17] S. X. Nakamura, A coupled-channel analysis of $D^+ \rightarrow K^- \pi^+ \pi^+$ decay, [arXiv:1504.02557](https://arxiv.org/abs/1504.02557).
 - [18] S. Weinberg, Phenomenological Lagrangians, *Ann. Phys. (N.Y.)* **96A**, 327 (1979).
 - [19] J. Gasser and H. Leutwyler, Chiral perturbation theory: Expansions in the mass of the strange quark, *Nucl. Phys.* **B250**, 465 (1985); , Chiral perturbation theory to one loop, *Ann. Phys. (N.Y.)* **158**, 142 (1984).
 - [20] G. Ecker, J. Gasser, A. Pich, and E. De Rafael, The role of resonances in chiral perturbation theory, *Nucl. Phys.* **B321**, 311 (1989).
 - [21] J. A. Oller and E. Oset, N/D description of two meson amplitudes and chiral symmetry, *Phys. Rev. D* **60**, 074023 (1999); , Chiral symmetry amplitudes in the S -wave isoscalar and isovector channels and the σ , $f_0(980)$, $a_0(980)$ scalar mesons, *Nucl. Phys.* **A620**, 438 (1997); **A652**, 407(E) (1999).
 - [22] G. Burdman and J. F. Donoghue, Union of chiral and heavy quark symmetries, *Phys. Lett. B* **280**, 287 (1992); M. B. Wise, Chiral perturbation theory for hadrons containing a heavy quark, *Phys. Rev. D* **45**, R2188 (1992).

- [23] D. R. Boito and M. R. Robilotta, Scalar resonances: Scattering and production amplitudes, *Phys. Rev. D* **76**, 094011 (2007).
- [24] J. H. Kühn and E. Mirkes, Structure functions in τ decays, *Z. Phys. C* **56**, 661 (1992) **67**, 364(E) (1995).
- [25] I. Bediaga, C. Gobel, and R. Mendez-Galain, Phenomenological analysis of nonresonant charm meson decays, *Phys. Rev. D* **56**, 4268 (1997).
- [26] R. Casalbuoni, A. Deandrea, N. Di Bartolomeo, R. Gatto, F. Feruglio, and G. Nardulli, Phenomenology of heavy meson chiral lagrangians, *Phys. Rep.* **281**, 145 (1997).
- [27] B. Hyams *et al.*, $\pi\pi$ Phase-shift analysis from 600 to 1900 MeV, *Nucl. Phys.* **B64**, 134 (1973).
- [28] K. A. Olive *et al.* (Particle Data Group), Review of Particle Physics, *Chin. Phys. C* **38**, 090001 (2014).
- [29] R. Higa and M. R. Robilotta, Two-pion exchange nucleon-nucleon potential: $O(q^4)$ relativistic chiral expansion, *Phys. Rev. C* **68**, 024004 (2003).
- [30] P. C. Magalhães, Ph.D. thesis, University of São Paulo, 2014.
- [31] G. Colangelo, J. Gasser, and H. Leutwyler, $\pi\pi$ scattering, *Nucl. Phys.* **B603**, 125 (2001).
- [32] P. C. Magalhães and M. R. Robilotta, Unitarization and low-energy scattering data, *Phys. Rev. D* **90**, 014043 (2014).
- [33] V. Bernard, N. Kaiser, and Ulf-G Meißner, πK scattering in chiral perturbation theory to one loop, *Nucl. Phys.* **B357**, 129 (1991).
- [34] P. Büttiker, S. Descotes-Genon, and B. Moussalam, A new analysis of πK scattering from Roy and Steiner type equations, *Eur. J. Phys.* **C33**, 409 (2004).